Synthesis, Crystal Structure Determination and Magnetic Study of a New [2 × 2] Grid Tetranuclear Fe(II) and Ni(II) Complexes Derived from the Ligand 1, 5-Bis(1-(Pyridin-2-Yl) Ethylidene) Carbonohydrazide)

Bocar Traoré [a], Thierno Moussa Seck [a], Mohamed Lamine Sall [a], Antoine Blaise Kama [b], Ousmane Diouf [a], Ibrahima El-Hadji Thiam [a] and Mohamed Gaye [a*]

[a] *Department of Chemistry, University Cheikh Anta DIOP de Dakar, Senegal.*
[b] *Department of Chemistry, University Alioune DIOP de Bambey, Senegal.*

Authors' contributions

This work was carried out in collaboration among all authors. All authors read and approved the final manuscript.

Original Research Article

Corresponding author: E-mail: mlgayeastou@yahoo.fr;

ABSTRACT

Complexes of nickel (II) and iron (III) are easily synthetized using the symmetrical ligand 1,5-bis(1-(pyridin-2-yl)ethylidene)carbonohydrazide) (H_2L) and metal nitrate salts. Square [2x2] grids structure of one tetranuclear iron and one tetranuclear nickel complex were isolated. X ray diffraction analysis reveals that the crystal structures of the two complexes are similar. The asymmetric unit of each complex consists of four cationic ligand molecules and four metal ions. Each ligand acts in its monodeprotonated form through five coordination sites such as two pyridine nitrogen atoms, two azomethine nitrogen atoms and one oxygen atom. Each of the four ligand molecules acts as a bridge between two metal ions yielding a square 2 x 2 grid structure. Each of the metal ion is hexacoordinated and is situated in a N_4O_2 core and the environment is best described as a severely distorted square bipyramidal geometry. Electrochemical studies show two electrons process for complex 1 and one electron process for complex 2. Variable temperature magnetic study shows that antiferromagnetic coupling is stronger in the nickel(II) than in the iron(II) complex. Perfect correlation between the magnetic properties and the crystallographic data are observed in both complexes.

1. INTRODUCTION

Chemists' interest in the self-assembly of transition metal ions with multifunctional organic ligands is continually growing [1-6]. Square and rectangular supramolecular grid structures continue to attract the interest of chemists, due to their potential applications in various scientific fields [7-10]. Square grid complexes [2×2], [3×3], [4×4] and [5×5] have been prepared and structurally characterized [11–20]. Among the multifunctional Schiff base ligands, those derived from carbohydrazide and thiocarbohydrazide are highly targeted for the design of novel grid structures [11–14, 17]. The presence of donor atoms such as nitrogen, oxygen, or sulfur in the structure of these ligands makes them able to bind several metal ions via μ-(N-N) and/or μ-O/μ-S bridges. However, the synthesis and characterization of a few square and rectangular grid transition metal complexes with those ligands have been reported [21–25]. Recently, a square grid $[Zn(HL)]_4 \cdot (NO_3)_4 \cdot 3H_2O$ (H_2L is 1,5-bis(1-(pyridin-2-yl)ethylidene)carbonohydrazide) has been reported by our research team in which the four Zn (II) centers are bridged by enoyl oxygen atoms [26]. Encouraged by these results, we continued investigations with the ligand 1,5-bis(1-(pyridin-2-yl)ethylidene)-carbonhydrazide as a building block for the self-assembly of novel transition metal ion grids structures [2 × 2]. Two grid square structures of were obtained when using the above ligand with iron(II) or nickel(II) nitrate salts. Herein, we report the crystal structure of $[Fe_4(HL)_4](NO_3)_4 \cdot 3H_2O$ (1) and $[Ni_4(HL)_4](NO_3)_4 \cdot 3H_2O$ (2) and their physico-chemical properties.

2. EXPERIMENTAL METHODS

2.1 Material and Physical Measurement

"Carbonohydrazide (98%), 2-acetylpyridine (99%), $Ni(NO_3)_2 \cdot 6H_2O$ (99%), $Fe(NO_3)_3 \cdot 9H_2O$ (99.99%) and methanol were supplied from Aldrich and used without further purification. All chemicals and solvents were used directly without further purification. The IR spectra were recorded on a Perkin Elmer Spectrum Two spectrophotometer (4000–400 cm^{-1}). The UV-Visible spectra was recorded on a Perkin Elmer Lambda UV-Vis spectrophotometer. The molar conductance of 10^{-3} M solution of the metal complexes in acetonitrile solutions were measured at 25 °C using a WTW LF-330 conductivity meter with a WTW conductivity. The voltammetric measurements were recorded using a Palm Sens3 type potentiostat controlled by PSTrace software. A glassy carbon working electrode with a radius of 2 ± 0.1 mm, a platinum wire as a counter-electrode and Ag/AgCl electrode as a reference were used. Cyclic voltammetry experiments were performed in acetonitrile solution 0.1 M of $LiClO_4$ as a supporting electrolyte" [26]. Magnetic measurements for complexes 1 and 2 were performed in the temperature range of 2–300 K by using a Cryogenic S600 SQUID magnetometer in an applied magnetic field of 1000 Oe. Raw data were corrected for the diamagnetism of the sample holder, measure in the same temperature and field range, and the intrinsic contribution of the sample, estimated by Pascal's constants.

2.2 Synthesis of the Ligand 1,5-bis(1-(pyridin-2-yl) ethylidene) Carbonohydrazide (H₂L)

Carbonohydrazide (2 g, 22.2 mmol) in 20 mL of methanol was stirred under reflux during 30 minutes before addition a solution of 2-acetylpyridine (10.75 g, 88.8 mmol) previously dissolved in 30 mL of methanol. The resulting mixture was stirred under reflux for 4 hours. On cooling a white precipitate appears from the uncolored solution. After filtration the precipitate was thoroughly washed with cold methanol and dried in desiccator over P_2O_5. A slow evaporation of a methanol solution of the compound gave crystal suitable for X-ray analysis. Yield: 41.1 %. M.p. = 195°C. ^{1}H NMR (250 MHz, DMSO-d_6, δ_H (ppm)): 2.3 (S, 6H, CH_3), 7.3 – 8.6(m, 8H, H_{Py}), 8.7 (S, 2H, N-H); 10.1 (S, 1H, O-H iminol). ^{13}C NMR (250 MHz, DMSO-d_6, δ_C, (ppm)): 155.4 (O-C=N), 153 (C=O), 152.1 (C_{Py}), 120.4 (C_{Py}), 137.0 (C_{Py}), 124.2 (C_{Py}), 149.1 (C_{Py}), 147.9 (C=N), 11.9 (CH_3), 22.8 (CH_3). FT-IR (ν, cm^{-1}): 3415, 3206, 1681, 1612, 1558, 1466, 1429, 1207, 1104. Anal. calcd. for $C_{15}H_{16}N_6O$: C, 60.80; H, 5.44; N, 28.36 %. Found: C, 60.78; H, 5.43; N, 28.32 %.

2.3 Synthesis of the Complex [Fe₄(HL)₄]·(NO₃)₄·2H₂O (1)

A mixture of $Fe(NO_3)_3 \cdot 9H_2O$ (0.25 mmol) and H_2L (0.25 mmol) in methanol (20 mL) was stirred at room temperature for one hour. The blood red solution was filtered, and the filtrate was kept at 298 K. After one week blood red crystals suitable for X-ray analysis appeared and were collected by filtration. Yield (%) = 39.46. FT-IR (ν, cm^{-1}) : 3461; 3157; 3075; 1617; 1572; 1546; 1464; 1357; 1317; 1201; 1157; 1011. UV-vis (solution, DMF,

λ, (nm)): 208; 288; 385; 475. Λ ($\Omega^{-1} \cdot cm^2 \cdot mol^{-1}$): 439.1 (fresh solution) and 441.3 (two weeks after). μ_{eff} (MB) = 9.89.

2.4 Synthesis of the Complex [Ni₄(HL)₄]·(NO₃)₄·4H₂O (2)

The above procedure was repeated: $Ni(NO_3)_2 \cdot 6H_2O$ was used instead $Fe(NO_3)_3 \cdot 9H_2O$. After one week blood red crystals suitable for X-ray analysis appeared and were collected by filtration. Yield (%) = 57.63. FT-IR (ν, cm^{-1}) : 3484; 3137; 3072; 1630; 1568; 1545; 1466; 1389; 1294; 1207; 1153; 1086. UV-vis (solution, DMF, λ (nm)): 211; 286; 383; 475; 790; 975. Λ ($\Omega^{-1} \cdot cm^2 \cdot mol^{-1}$): 438.1 (fresh solution) and 440.3 (two weeks after). μ_{eff} (MB) = 5.75.

2.5 X-ray Data Collection, Structure Determination and Refinement

Details of the X-rays crystal structure solution and refinement are given in Table 1. Diffraction data were collected using a Bruker APEX-II CCD diffractometer with graphite monochromatized MoKα radiation (λ = 0.71073 Å) for the complex (1) and Super Nova, Dual, Cu at home/near, AtlasS2 diffractometer with graphite monochromatized CuKα radiation (λ = 1.54184 Å) for the complex (2). All data were corrected for Lorentz and polarization effects. No absorption correction was applied. Complexes scattering factors were taken from the program package SHELXTL solution and refinement were performed using *SHELXT* [27] and *SHELXL*-2014/7 [28]. All hydrogen atoms were added in calculated positions and refined in riding mode on the parent atom. Molecular graphics were generated using *ORTEP-3* [29].
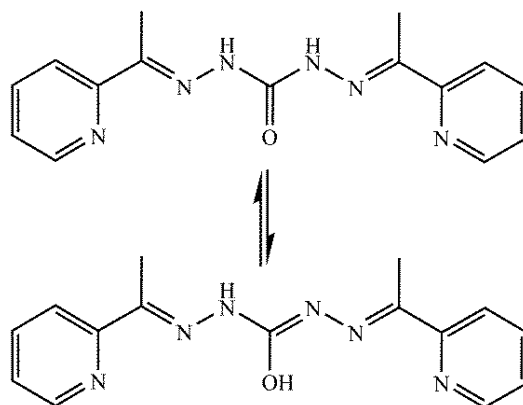

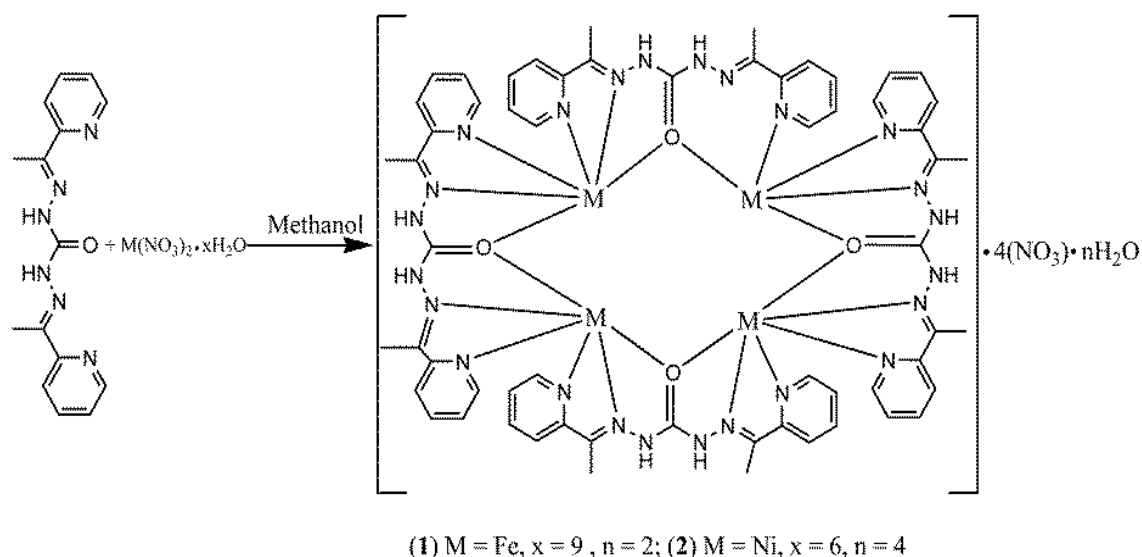**Diagram 1 . Keto-enol equilibrium of H₂L in DMSO solution**

(1) M = Fe, x = 9 , n = 2; (2) M = Ni, x = 6, n = 4

Diagram 2. Synthetic scheme for complexes 1 and 2

Table 1. Crystal data and data collection details of the complexes (1) and (2)

Empirical formula	$C_{60}H_{60}N_{24}O_4Fe_4 \cdot 4(NO_3) \cdot 2(H_2O)$ (1)	$C_{60}H_{60}N_{24}O_4Ni_4 \cdot 4(NO_3) \cdot 4(H_2O)$ (2)
Formula weight (g/mol)	1697.63	1729.28
T (K)	293(2)	293(2)
Radiation	Mo Kα (λ = 0.71073 Å)	CuKα (λ = 1.54184 Å)
Crystal system	Tetragonal	Tetragonal
Space group	I4$_1$/a	I-42d
Z	36	16
a (Å)	13.8395 (4)	13.63430(10)
b (Å)	13.8395 (4)	13.63430(10)
c (Å)	35.8385 (10)	40.4899(4)
Volume (Å^3)	6864.2 (3)	7526.84(13)
D_{cal} (g cm^{-3})	1.626	1.526
μ(mm^{-1})	0.922	1.873
Crystal size/mm^3		0.4 × 0.24 × 0.22
F(000)	3447.2	3572.0
θ$_{max}$ (°)	29.5	71.03
h, k, l range	-10 ≤ h ≤ 18; -18 ≤ k ≤ 7; -45 ≤ l ≤ 27	-14 ≤ h ≤ 16; -16 ≤ k ≤ 16; -49 ≤ l ≤ 49
Measured reflections	11710	63061
Independant Reflections	4107	3638
Reflections [I > 2σ(I)]	3130	3420
Rint	0.034	0.0279
Goodness-of-Fit	1.02	1.118
R 1[I > 2σ(I)]	R$_1$ = 0.0526	0.0364
wR$_2$	0,127	0.1095
Data/parameters/restraints	4107/271/0	3638/38/302
Δρ$_{max}$, min (e Å^{-3})	0.99/-0.77	0.44/-0.27

3. RESULTS AND DISCUSSION

3.1 General Studies

The ^{1}H and ^{13}C NMR spectra of H_2L recorded in DMSO-d_6 reveal a partial iminolisation of the ligand in dmso solution (Diagram 1). A broad singlet appearing at 10.1 ppm is attributed to the H–O proton of the iminol function. Two signals pointed a 155.4 ppm (O–C=N) and 153 ppm (N–C=O) are indicative of the simultaneous presence of the iminol and the keto forms in solution. Additionally, two signals at 11.9 ppm and 22.8 ppm attributable to the carbon atoms of the –CH$_3$ groups are indicative of a dissymmetric nature of the molecule after the iminolization. The IR spectrum of the ligand shows bands at 3415 cm^{-1}, 3206 cm^{-1}, 1681 cm^{-1} and 1612 cm^{-1}, which are, respectively, assigned to $\nu_{O–H}$, $\nu_{N–H}$, $\nu_{C=O}$ and $\nu_{C=N}$ [30]. The bands due to the pyridine ring appear in the range 1558-1466 cm^{-1}. Upon coordination the FT-IR spectra of complexes **1** and **2** (Diagram 2) show a shift for the band due to C=O and C=N. For complex (**1**) $\nu_{C=O}$ and $\nu_{C=N}$ are pointed, respectively, at 1617 cm^{-1} and 1572 cm^{-1}. For complex (**2**) those bands are pointed at 1630 cm^{-1} and 1568 cm^{-1}. These shifts to low frequencies indicate the involvement of the carbonyl oxygen atom and the azomethine nitrogen atom to the coordination. Additionally, the shift to low frequencies of the bands due to the pyridine ring confirms the coordination of the pyridine nitrogen atom. The sharp and strong band which appears at 1380 cm^{-1} in both

infrared spectra of the two complexes is attributed to the free nitrate group. The electronic spectrum of the iron (II) complex in acetonitrile solution shows three main bands at 288 nm, 385 nm, and 475 nm attributable, respectively, attributed to $\pi \rightarrow \pi^*$, $n \rightarrow \pi^*$ of the ligand and to the ligand-metal charge transfer band. In the UV-vis spectrum of the nickel (II) complex, besides the intra-ligand bands we observe two bands at 790 nm and 975 nm. These bands correspond to the $d \rightarrow d$ transitions which are characteristic of octahedral geometry around Ni(II) cation. The molar conductivities of the fer (II) complex and the nickel (II) complex are measured for a freshly prepared acetonitrile solution and after two weeks of standing. These values are, respectively, 439.1 and 441.3 $\Omega^{-1} \cdot cm^2 \cdot mol^{-1}$ for the iron(II) complex and 438.1 and 440.3 $\Omega^{-1} \cdot cm^2 \cdot mol^{-1}$ for the for nickel (II) complex, indicating electrolyte of type 4:1 [31] and good stability of these complexes in acetonitrile.

3.2 Description of the Structures

Suitable single-crystals for X-ray diffraction of the Fe(II) and Ni(II) complexes were obtained by slow solvent evaporation at room temperature. Crystal data, collection and refinement parameters are listed in Table 1. Selected bond lengths and angles are summarized in Table 2. Figs. 1-2 and Figs. 4-5 displays, respectively, the asymmetric unit and the packing diagrams of the two compounds.
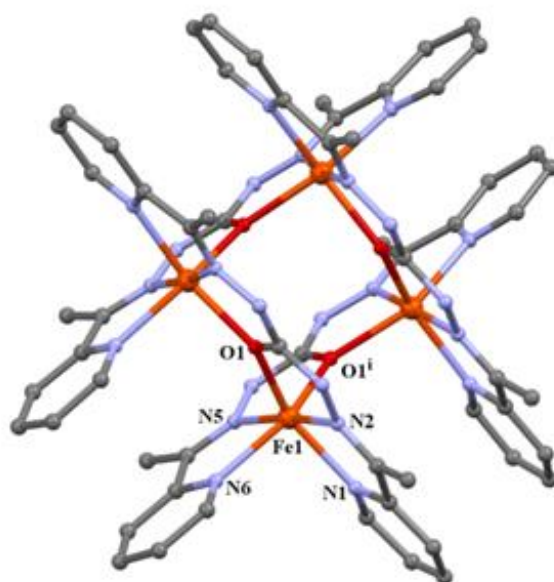

Fig. 1. ORTEP plot (30% probability ellipsoids) showing the molecule structure of the Fe[II]
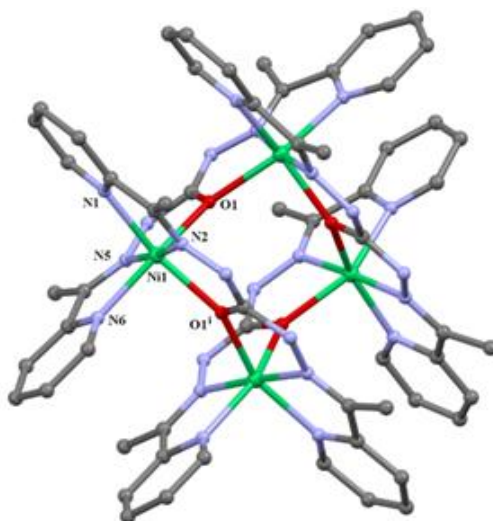
Fig. 2. ORTEP plot (30% probability ellipsoids) showing the molecule structure of the Ni[II]

Table 2. Selected bond lengths (A) and angles (°) for the complex 1

1			
Fe1—O1^i	2.1155 (16)	Fe1—N5^i	2.098 (2)
Fe1—O1	2.1057 (16)	Fe1—N6^i	2.177 (2)
Fe1—N2	2.104 (2)	Fe1—N1	2.149 (2)
O1—Fe1—O1^i	95.17 (9)	N2—Fe1—N1	74.51 (8)
O1i—Fe1—N6^i	148.39 (7)	N5i—Fe1—O1^i	74.31 (7)
O1—Fe1—N6^i	94.70 (7)	N5i—Fe1—O1	107.87 (7)
O1^i—Fe1—N1	93.08 (7)	N5^i—Fe1—N2	172.63 (9)
O1—Fe1—N1	148.17 (7)	N5^i—Fe1—N6^i	74.08 (8)
N2—Fe1—O1^i	112.84 (7)	N5^i—Fe1—N1	103.96 (8)
N2—Fe1—O1	73.95 (7)	N1—Fe1—N6^i	94.16 (8)
N2—Fe1—N6^i	98.74 (8)	Fe1—O1—Fe1^{ii}	131.02 (7)

Symmetry codes: (i) −y+3/4, x−1/4, −z+3/4; (ii) y+1/4, −x+3/4, −z+3/4.

Table 3. Selected bond lengths (Å) and angles (°) for the complex 2

2			
Ni1—O1^i	2.097 (2)	Ni1—N2	1.982 (3)
Ni1—O1	2.109 (2)	Ni1—N5^i	2.002 (3)
Ni1—N1	2.091 (3)	Ni1—N6^i	2.079 (3)
O1^i—Ni1—O1	90.60 (11)	N5^i—Ni1—O1^i	77.18 (10)
N1—Ni1—O1	155.02 (10)	N5^i—Ni1—O1	109.33 (10)
N1—Ni1—O1^i	93.37 (10)	N5^i—Ni1—N1	95.59 (11)
N2—Ni1—O1	76.35 (10)	N5^i—Ni1—N6^i	77.48 (12)
N2—Ni1—O1^i	102.75 (10)	N6^i—Ni1—O1	91.08 (10)
N2—Ni1—N1	78.72 (11)	N6^i—Ni1—O1^i	153.68 (10)
N2—Ni1—N5^i	174.31 (12)	N6^i—Ni1—N1	96.09 (11)
N2—Ni1—N6^i	103.17 (12)	Ni1^{ii}—O1—Ni1	137.64 (10)

Symmetry codes: (i) −y+1, x, −z+1; (ii) y, −x+1, −z+1.

The tetranuclear iron(II) (1) and (Ni(II) (2) complexes crystallize in the tetragonal space group I4$_1$/a. The molecular structures of the complexes 1 and 2 with the atomic numbering scheme are illustrated in Figs. 1 and 2, respectively. Selected bond distances and angles are listed in Tables 2 and 3. The complexes consist of a 2 x 2 square grid formed with four metal (II) ions bridged by four monodeprotonated ligand (HL⁻). Four nitrate

anions and two (1) or four (2) uncoordinated water molecules are present in the asymmetric unit. The two complexes 1 and 2 are isostructural. Four metal ions and four organic monodeprotonated ligand form a 2 x 2 grid structure. The pentadentate organic ligand acts in its *syn*-conformation form through the two azomethine nitrogen atoms, the two pyridine nitrogen atoms, and the carbonyl oxygen atom which acts as bridge between two metal ions. The bridging angles are Fe—O—Fe [131.02(7)°] and Ni—O—Ni [137.64(10)°]. Each metal ion is situated in a N_4O_2 core and the environments around the metal ions are best described as a strongly distorted octahedral geometries (Figs. 3a and 3c). The equatorial planes are occupied by the N1, N6, O1 and O1^i atoms while the N2 and N5^i atoms occupy the apical positions in each structure. The values of the *cissoid* angles in the equatorial plane vary between 93.08(7)° and 95.17(9)° for complex 1 and 91.10(11)° and 96.09(11)° for complex 2. The *transoid* angles are 148.17(7)° and 148.39(7)° for complex 1 and 153.68(10)° and 155.02(10)° for complex 2. The angle defined by the atoms occupying the axial positions are 172.63(9)° (1) and 174.31(12)° (2). These angle values deviated severely from the ideal values of 90° and 180° expected for octahedral environment. The adjacent Fe(II) in (1) and Ni(II) in (2) ions are bridged by the oxygen atom of their shared ligand. The Fe—O distances [2.1057(16 Å and 2.1155(16) Å] and Ni—O [2.097(2) Å and 2.109(2) Å] are comparable to the values found for similar complexes [32, 33].

The bond lengths of Fe—N_{Py} [2.149(2) Å and 2.177(2) Å] are longer than the distances of Ni—N_{Py} [2.079(3) Å and 2.091(3) Å]. The distances Fe—Fe [3.8413(6) Å] and Ni—Ni [3.9218(8) Å] are compatible with the presence of interaction between metal centers. The oxygen atoms are situated alternatively up [0.868 Å] and down [0.868 Å] of the mean plane formed by the four iron(II) giving a boat-like arrangement as shown in Fig. 3b. The same facts are observed in the nickel(II) complex. The oxygen atoms are situated alternatively up [0.743 Å] and down [0.743 Å] of the mean plane formed by the four nickel(II) giving a boat-like arrangement as shown in Fig. 3d. The [2 x 2] grid for the complex 1 is not perfectly square as can be seen by the dihedral angles involving the mean planes defined by adjacent hydrazone moieties [89.85°] and the dihedral angle value of 5.85° between the mean planes defined by the opposite hydrazone moieties. In complex 2 the dihedral angle between the mean planes defined by

adjacent hydrazone moieties [89.82°] and the dihedral angle [6.47°] between the opposite mean planes defined by hydrazone moieties show that the [2 x 2] grid is not perfectly square. The supramolecular structure of the two complexes (1) and (2) shows a chains of molecules linked by numerous intermolecular hydrogen bonds of type C—H···ONO_2 and C—H···OH_2 (Tables 4 and 5). Intermolecular hydrogen bond of type $N_{hydrazino}$—H···ONO_2 are also observed in both structures (Figs. 3 and 4). In the complex 1, intramolecular hydrogen bond of type $N_{hydrazino}$—H···ONO_2 and C—H···ONO_2 consolidate the structure (Fig. 3, Table 4).

3.3 Electrochemistry Study

The electrochemical properties of tetranuclear square grids iron (II) and nickel (II) complexes were studied by cyclic voltammetry using a carbon graphite working electrode auxiliary to platinum wire in acetonitrile and lithium perchlorate as supporting electrolyte. The voltammeter parameters were studied in the sweep frequency range 10-300 mV·S^{-1}. The voltammograms of the complexes presented in Figs. 6-9 respectively, were recorded between -300 to 300 V with a scan rate of 100 mV/S in acetonitrile. On the cyclic voltammogram of the iron (II) complex (**1**), the anodic part shows two oxidation peaks at potentials 1.201 V and 1.424 corresponding to dielectronic processes $Fe^{II}Fe^{II}Fe^{II}Fe^{II}$ → $Fe^{II}Fe^{II}Fe^{III}Fe^{III}$ → $Fe^{III}Fe^{III}Fe^{III}Fe^{III}$. The cathodic part reveals two reduction peaks at potentials -1.013 V and -1.322 V corresponding to the dielectronic processes $Fe^{III}Fe^{III}Fe^{III}Fe^{III}$→$Fe^{III}Fe^{III}Fe^{II}Fe^{II}$→ $Fe^{II}Fe^{II}Fe^{II}Fe^{II}$. Analysis of the cyclic voltammogram of the nickel(II) complex reveals four reduction peaks at potentials 0.395 V, -0.441 V, -1.332 V and -1.794 V corresponding to the single-electron processes $Ni^{II}Ni^{II}Ni^{II}Ni^{II}$ → $Ni^{II}Ni^{II}Ni^{II}Ni^{I}$ → $Ni^{II}Ni^{II}Ni^{I}Ni^{I}$→$Ni^{II}Ni^{I}Ni^{I}Ni^{I}$→ $Ni^{I}Ni^{I}Ni^{I}Ni^{I}$ and four oxidation peaks at potentials 1.531 V, 0.689 V, -1.019 V and -1.649 V corresponding to the single-electron processes $Ni^{I}Ni^{I}Ni^{I}Ni^{I}$ → $Ni^{II}Ni^{I}Ni^{I}Ni^{I}$ →$Ni^{II}Ni^{II}Ni^{I}Ni^{I}$ → $Ni^{II}Ni^{II}Ni^{II}Ni^{I}$ → $Ni^{II}Ni^{II}Ni^{II}Ni^{II}$. The kinetic study on the oxidation and reduction of the two complexes with different scan rates shows an increase in the intensity of the oxidation and reduction peaks with increasing scan rate. The ratios of the anodic peak current to the cathodic peak current tend towards unity indicating a reversibility of the redox processes in both complexes.
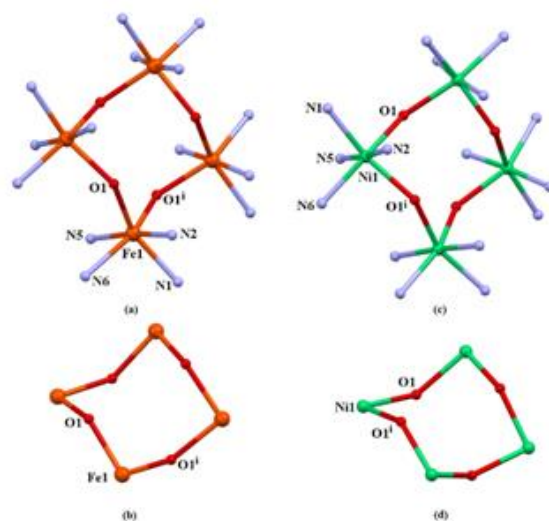
Fig. 3. Plot showing the environment around the Fe(II) (a) and Ni(II) (c) ions and boat-like arrangement formed by the four Fe(II) ions (b) and by the four Ni(II) ions (d)

Table 4. Hydrogen bond geometry (Å, °) in complex 1

D—H⋯A	D—H	H⋯A	D⋯A	D—H⋯A
N4—H4⋯O3	0.86	2.01	2.783(5)	149.3
C1—H1⋯O3ⁱⁱⁱ	0.93	2.47	3.324(5)	152.1
C1—H1⋯N3B^{iv}	0.93	2.63	3.358(6)	135.4
C1—H1⋯O2^{iv}	0.93	2.66	3.256(5)	122.9
C10—H10A⋯O3	0.96	2.48	3.395(7)	160.0
C10—H10B⋯O5^v	0.96	2.43	3.342(6)	159.2
C10—H10C⋯N3^{vi}	0.96	2.55	3.432(4)	152.3
C4—H4A⋯N7^{vii}	0.93	2.65	3.314(3)	128.8
C4—H4A⋯O4^{viii}	0.93	2.52	3.293(5)	140.8
C4—H4A⋯O6^{vii}	0.93	2.41	3.272(5)	154.9
C14—H14⋯O6	0.93	2.55	3.210(5)	128.4
C7—H7A⋯O4ⁱ	0.96	2.55	3.501(6)	168.5
C7—H7C⋯O2^{ix}	0.96	2.53	3.475(6)	169.8
C12—H12⋯O4^v	0.93	2.52	3.372(5)	153.2
C2—H2⋯O2ⁱⁱⁱ	0.93	2.42	3.073(6)	127.1

Symmetry codes: (i) −y+3/4, x−1/4, −z+3/4; (iii) y+1/4, −x+5/4, z+1/4; (iv) −y+3/4, x+1/4, z+1/4; (v) y+3/4, −x+3/4, z−1/4; (vi) −x+3/2, −y+1/2, −z+1/2; (vii) −y+1/4, x−1/4, z−1/4; (viii) y+1/4, −x+7/4, −z+3/4; (ix) −x+1, −y+1/2, z.

Table 5. Hydrogen bond geometry (Å, °) in complex 2

D—H⋯A	D—H	H⋯A	D⋯A		D—H⋯A
N4—H4⋯O3ⁱ	0.86	1.99	2.784	(8)	154.1
N4—H4⋯O8ⁱ	0.86	2.28	3.068	(12)	152.7
C4—H4A⋯O5ⁱⁱⁱ	0.93	2.45	3.287	(13)	149.5
C7—H7A⋯O7ⁱⁱⁱ	0.96	2.52	3.320	(12)	140.5
C14—H14⋯O2^{iv}	0.93	2.61	3.285	(7)	130.2
C14—H14⋯O4^{iv}	0.93	2.48	3.274	(13)	143.6
C15—H15C⋯O3ⁱ	0.96	2.64	3.254	(14)	122.4
O9—H9A⋯O4^v	0.85	2.28	2.967	(16)	138.3

Symmetry codes: (i) −y+1, x, −z+1; (iii) −y+1, −x+3/2, z+1/4; (iv) −x+3/2, y, −z+3/4; (v) x−1/2, −y+1, −z+3/4
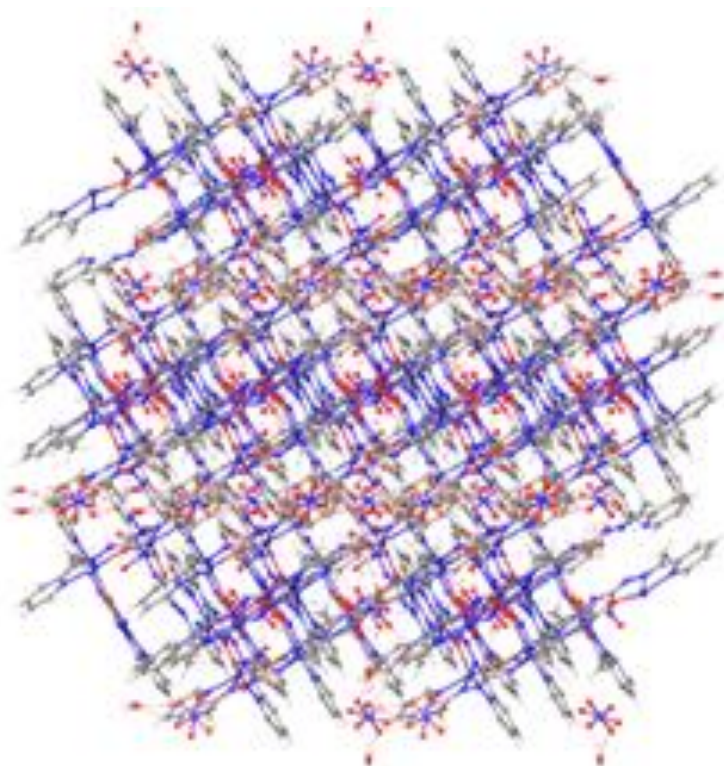
Fig. 4. View of the chains formed by hydrogen bonds in the ac plane (1)
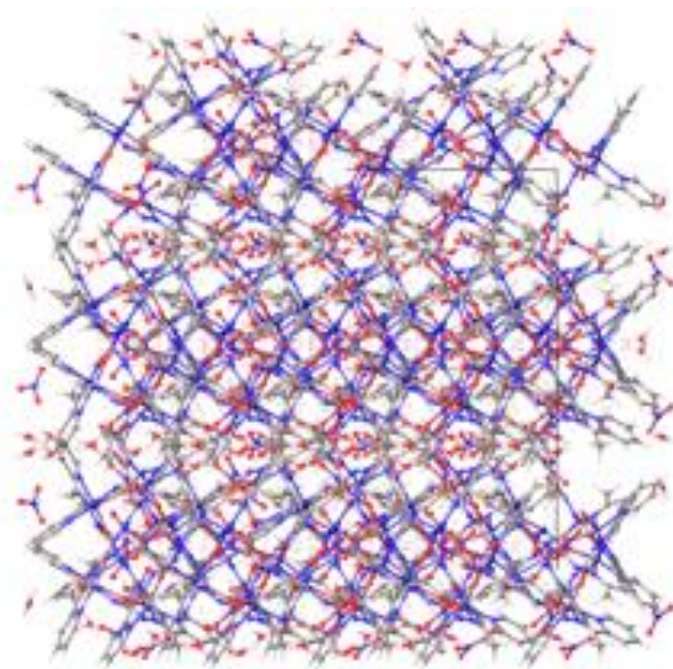

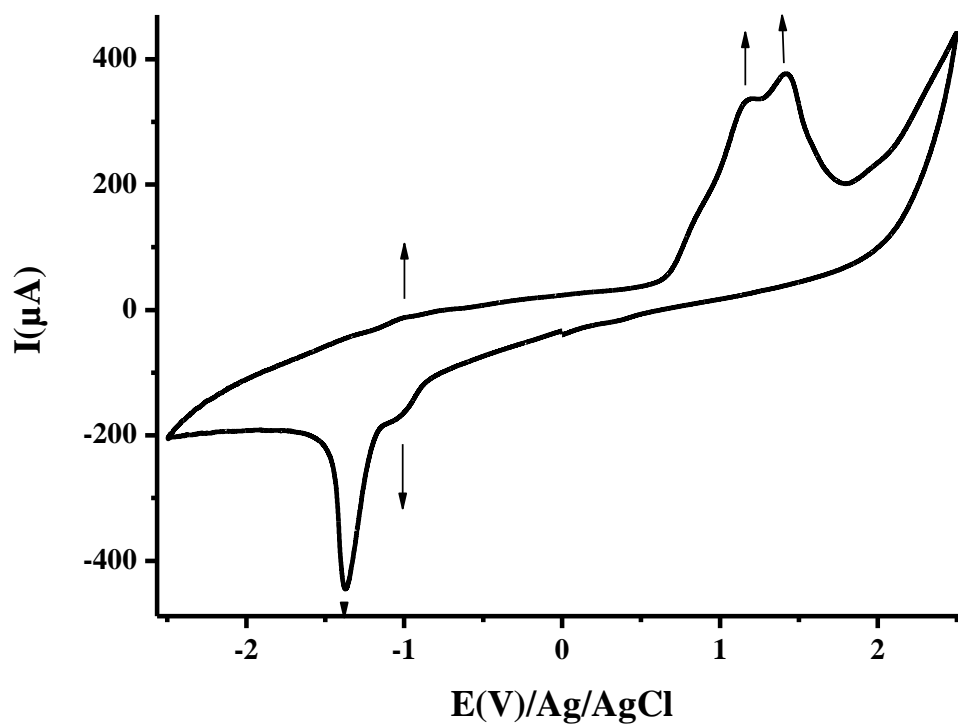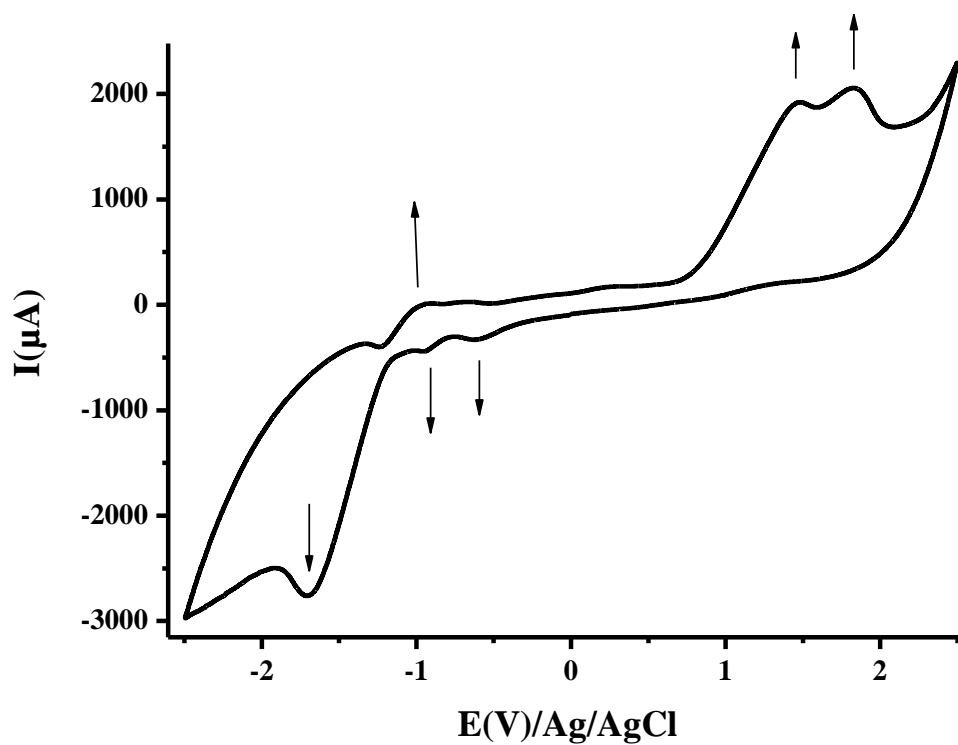**Fig. 5. View of the chains formed by hydrogen bonds in the bc plane (2)**
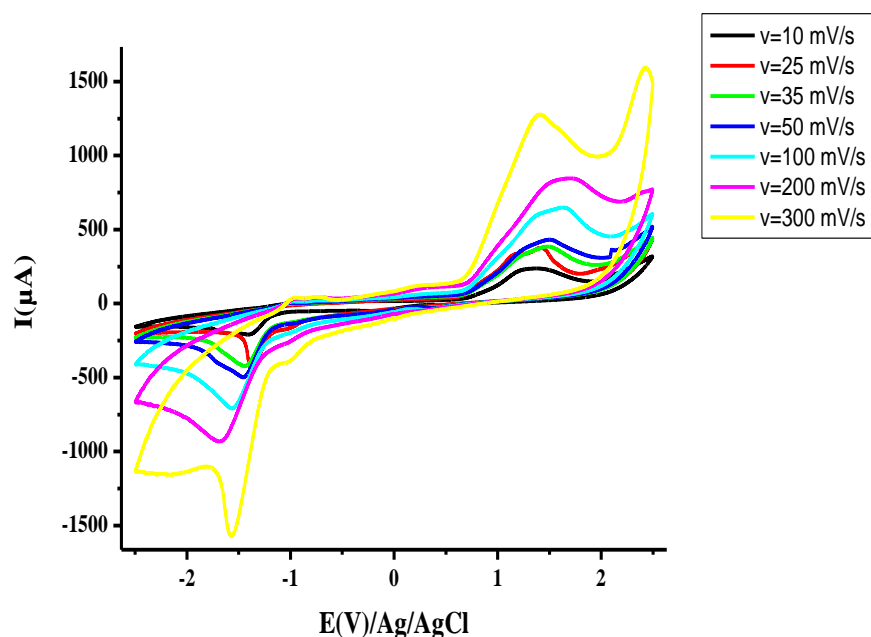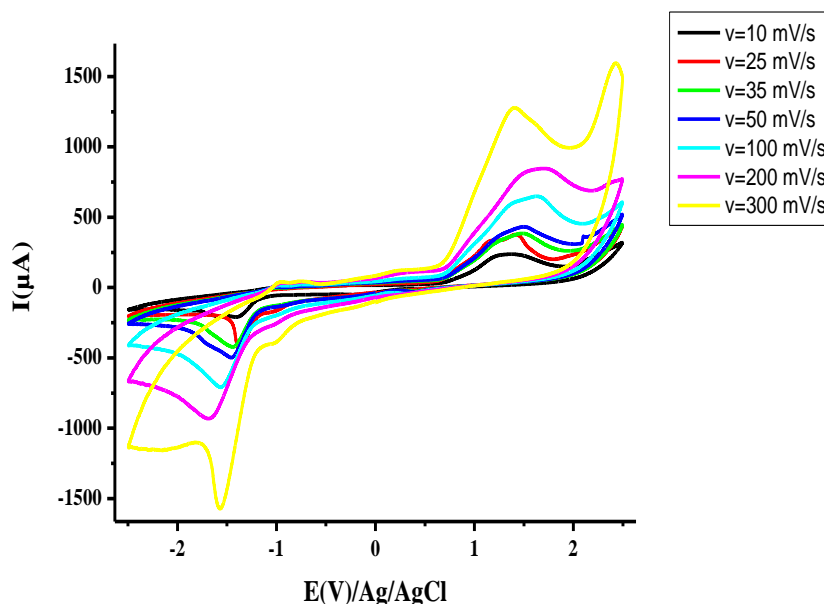
Fig. 6. Cyclic Voltammogram of the complex 1 in CH$_3$CN containing 0.1 M LiClO$_4$. Working electrode: 2 mm diameter of graphite carbon electrode, scan rate: 25 m·Vs^{-1}

Fig. 7. Cyclic Voltammogram of the complex 2 in CH$_3$CN containing 0.1 M LiClO$_4$. Working electrode: 2 mm diameter of graphite carbon electrode, scan rate: 500 m·Vs^{-1}

Fig. 8. Cyclic Voltammograms of the complex 1 in CH₃CN containing 0.1 M LiClO₄. Working electrode: 2 mm diameter of graphite carbon electrode scan rate: 10, 25, 50, 100, 200 and 300 mVs⁻¹

Fig. 9. Cyclic Voltammograms of the complex 2 in CH₃CN containing 0.1 M LiClO₄. Working electrode: 2 mm diameter of graphite carbon electrode scan rate: 10, 25, 50, 100, 200 and 300 mVs⁻¹

3.4 Magnetic Property Of Complex $[Fe_4(HL)_4] \cdot (NO_3)_4 \cdot 2H_2O$

The dependence of the magnetic susceptibility on the temperature of the tetranuclear iron (II) complex (1) was measured in the temperature range 300-2 K with an applied field of 1000 Oe. The magnetic susceptibility varies weakly in the temperature range 300 – 100 K and grows faster below 100 K by tending asymptotically towards the ordinate axis at low temperature (Fig. 10). To elucidate the magnetic properties of the complex

(1) we have drawn the curve of the product of molar susceptibility with temperature as a function of the latter: χT *vs* T (Fig. 11). The value χT is almost constant between 200 K and 300 K and at room temperature it is equal at 10.69 cm^3·K·mol^{-1}. This value is lower than 12.004 cm^3·K·mol^{-1}, expected for four iron (II) without magnetic interaction with S = 3/2 and g = 2. This large difference is due to the presence of an antiferromagnetic interaction within the complex. The curve of the variation of $1/\chi$ *vs* T (Fig. 12) shows that the magnetic susceptibility data in the range of 25-300 K fits the Curie-Weiss law, χ = C / (T - θ), with Curie constant C = 11.69 cm^3 mol^{-1} K^{-1} and negative Weiss constants θ of - 27.55 K, which indicates the antiferromagnetic exchange coupling between the Fe (II) ions. The evolution of the magnetization as a function of the magnetic field of the complex 1 at 2 K shows an increase in the magnetization and tends towards a value of 4.505 Nβ at 70 kOe (Fig. 13).

This value is far from the saturation value for four high spin Fe(II). This shift could be due to Zero field splitting and anisotropy phenomena. The magneto-structural study shows a perfect correlation between the crystallographic data and the magnetic properties of complex 1. The distances between two adjacent iron (II) ions and two diagonal iron (II) ions measure respectively 3.841 Å and 5.415 Å. The distance 3.841 Å is close to that observed in an iron (II) tetranuclear complex exhibiting an antiferromagnetic interaction between adjacent iron (II) ions [34]. The distance 5.415 Å is greater than that observed between two iron ions (II) without interaction. This remark allows us to neglect the magnetic interaction between the diagonal iron (II) ions (Fig. 14). The bridging Fe—O—Fe angle value of 131.06° agrees with the antiferromagnetic coupling observed within complex 1 [35].
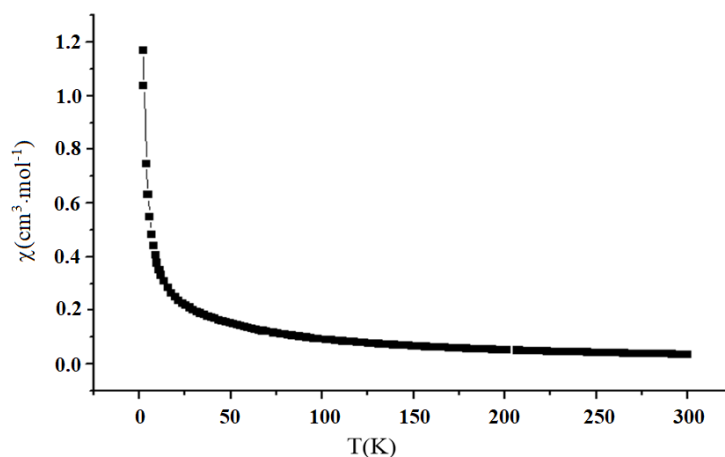

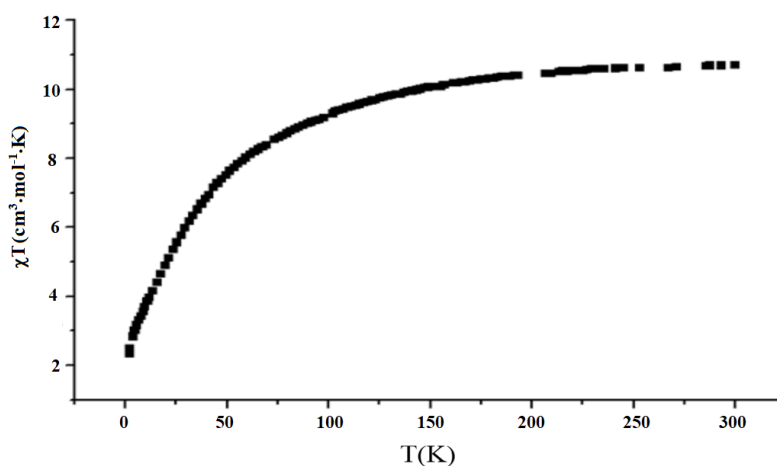**Fig. 10. Experimental variations of χM versus T for complex 1 at 1000 Oe**

Fig. 11. Experimental variations of χMT versus T for complex 1 at 1000 Oe
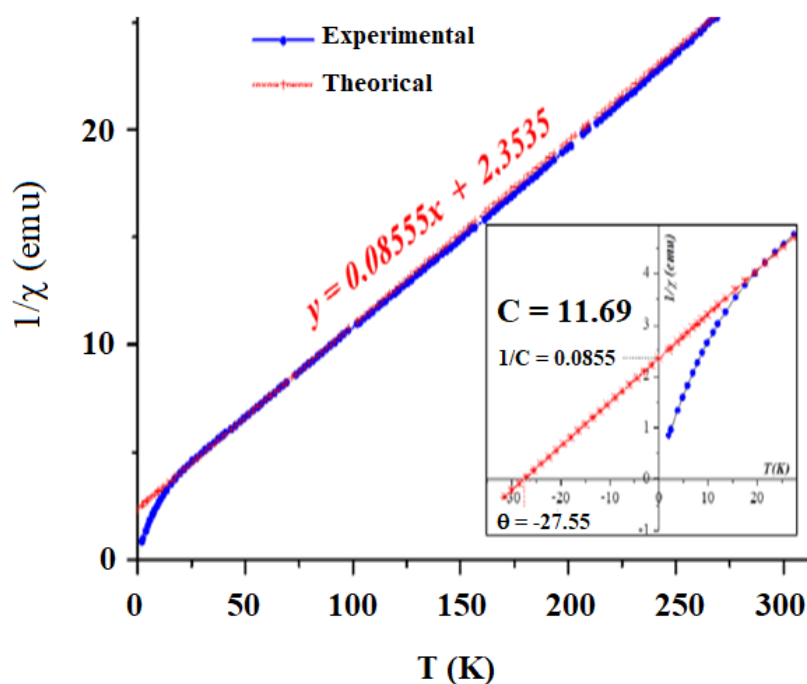
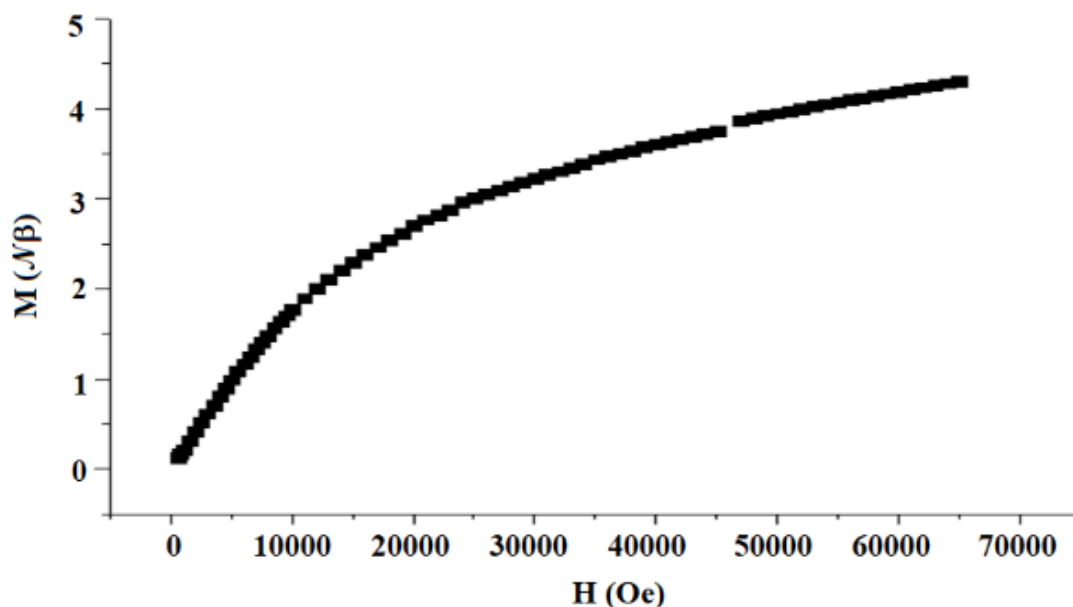**Fig. 12. Experimental variations of 1/χ versus T for complex 1 at 1000 Oe**

Fig. 13. Isothermal magnetization of 1 at 2 K

3.5 Magnetic property of complex [Ni$_4$(HL)$_4$]·(NO$_3$)$_4$·4H$_2$O

The magnetic properties of the compound 2 have been investigated in the temperature range 2−300 K an applied field of 1000 Oe on powdered microcrystalline samples with a SQUID magnetometer. For the complex 2 a decrease of the product χT with cooling is observed. This decay is the manifestation of an antiferromagnetic interaction in accordance with the crystallographic structure. The value of product χT (4.13 cm^3·K·mol^{-1}) at room temperature (Fig. 15) is lower than the expected

value of 5.06 cm^3·K·mol^{-1} for four nickel(II) ions without interaction for a gyromagnetic constant g = 2.248. This shift confirms the antiferromagnetic coupling between the nickel (II) ions. Fig. 16 represents the evolution of magnetic susceptibility *vs* the temperature. It shows that the magnetic susceptibility increases with cooling from 0.015 cm^3·mol^{-1} to 0.042 cm^3·mol^{-1} in the range 300-14 K and subsequently decreases very rapidly to 0.005 cm^3·mol^{-1}. The presence of a maximum at Neel temperature (TN = 41 K) is a characteristic of a strong intramolecular antiferromagnetic coupling. It is established by previous studies that the value of the bridging angle Ni—O—Ni is an important parameter in the magneto-structural correlation [36, 37]. The Ni—O—Ni bridging angle which is 137.6(1)° is well correlated with the antiferromagnetic interactions for complex 2.
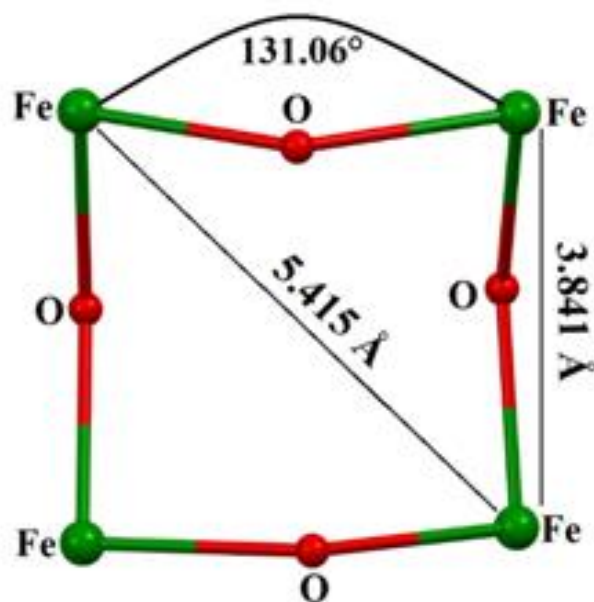

Fig. 14. square grid with structural parameters that can influence the magnetic properties of the complex 1
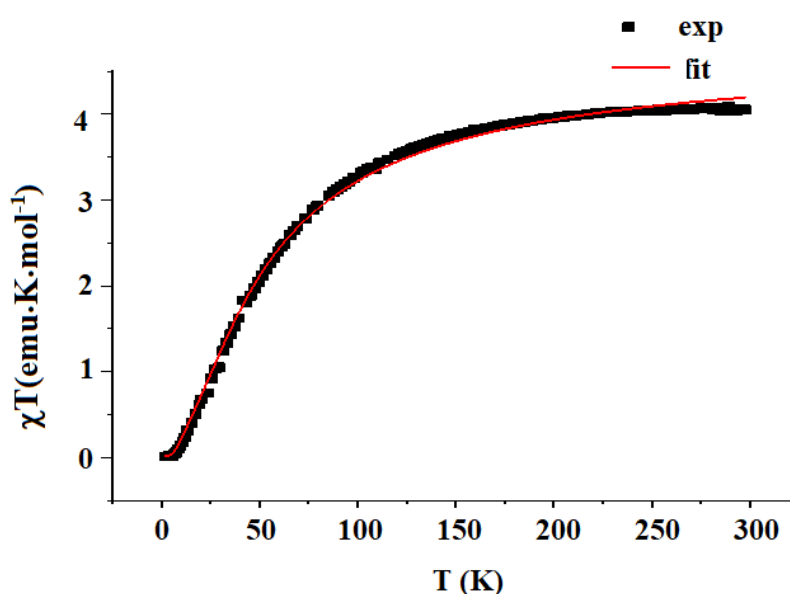

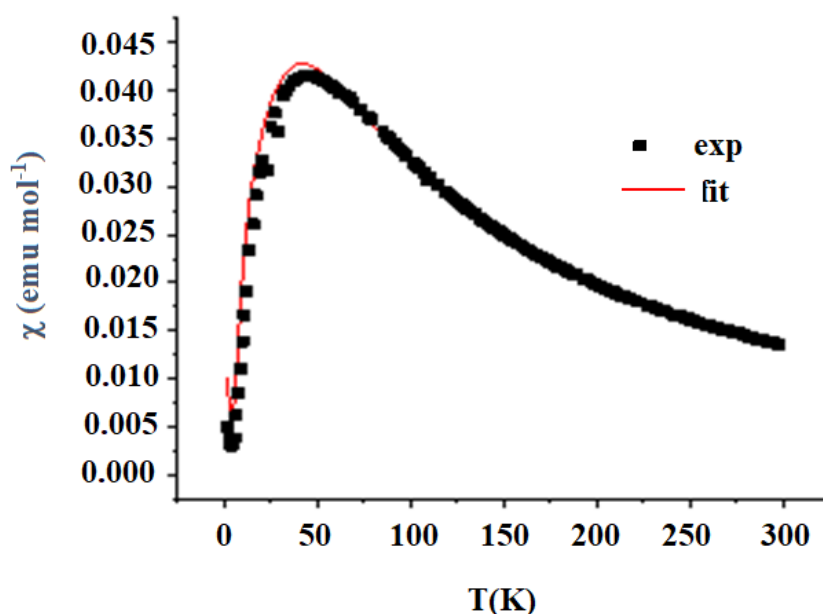**Fig. 15. Experimental variations of χMT versus T for complex 2 at 1000 Oe**

Fig. 16. Experimental variations of χM versus T for complex 2 at 1000 Oe

4. CONCLUSION

Tetranuclear square [2 × 2] homodivalent Fe(II) and Ni(II) grid complexes comprising symmetric picolinic hydrazone-based ligand have been synthesized. The complexes are fully characterized by infrared and UV-Visible spectroscopies, molar conductivity measurement, electrochemistry study, single crystal XRD and magnetic property analysis. The complexes are formulated as $[Fe_4(HL)_4]\cdot(NO_3)_4\cdot2H_2O$ and $[Ni_4(HL)_4]\cdot(NO_3)_4\cdot4H_2O$. All the metal centers are situated in strongly distorted octahedral environment. Both complexes show antiferromagnetic coupling with a best intensity coupling in complex 2. The magneto-structural study showed a perfect correlation between the crystallographic data and the magnetic properties. The electrochemical study showed a two electronic process for complex 1 and one electronic process for the complex 2.

AVAILABILITY OF DATA

CCDC-2282038 (**1**) and 2282039 (**2**) contain the supplementary crystallographic data for this paper. These data can be obtained free of charge via https://www.ccdc.cam.ac.uk/structures/, or by emailingdata_request@ccdc.cam.ac.uk, or by contacting The Cambridge Crystallographic Data Centre, 12 Union Road, Cambridge CB2 1EZ, UK.

COMPETING INTERESTS

Authors have declared that no competing interests exist.

REFERENCES

1. Seck TM, Gueye MN, Thiam IE, Diouf O, Gaye M, Retailleau P. Synthesis, Spectroscopic and X-Ray Structure Determination of a New Mononuclear Terbium (III) Complex from the Ligand *N,N'*-1,5-bis(pyridylmethylidene) Carbonohydrazone (H₂L). Earthline J. Chem. Sci. 2022;9(1):121–137. Available:https://doi.org/10.34198/ejcs.912 3.121137

2. Seck TM, Gaye PA, Diouf O, Thiam IE, Gaye M. Synthesis, Spectroscopic Studies and Crystal Structure Determination of a Novel Mn(II) Complex with N,N-1,5-bis(2-acetylpyridinyl)carbonohydrazone Ligand. Chem. Afr. 2020;3(4):949–954. Available:https://doi.org/10.1007/s42250-020-00140-9

3. Hashim KKM, Manoj E, Kurup MRP. A novel manganese(II) bisthiocarbohydrazone complex: Crystal structures, Hirshfeld surface analysis, DFT and molecular docking study with SARS-CoV-2. J. Mol. Struct. 2021;1246:131125. Available:https://doi.org/10.1016/j.molstruc. 2021.131125

4. Anwar MU, Thompson LK, Dawe LN, Habib F, Murugesu M. Predictable self-assembled [2 × 2] Ln(III)$_4$ square grids (Ln = Dy,Tb)—SMM behaviour in a new lanthanide cluster motif. Chem. Commun. 2012;48(38):4576–4578.
Available https://doi.org/10.1039/C2CC17546K

5. Bikas R, Hosseini-Monfared H, Siczek M, Demeshko S, Soltani B, Lis T. Synthesis, structure, and magnetic properties of a tetranuclear Mn(II) complex with carbohydrazone based ligand. Inorg. Chem. Commun. 2015;62:60–63.
Available:https://doi.org/10.1016/j.inoche.2015.10.021

6. Zhang, L, Wang, J-J, Xu, G-C. (2014). The [2×2] grid tetranuclear Fe(II) and Mn(II) complexes: Structure and magnetic properties. Inorg. Chem. Commun. 2014;39:66–69.
Availablehttps://doi.org/10.1016/j.inoche.2013.10.048

7. Ashebr TG, Li, X-L, Zhao C, Yang Q, Tang, J. (2022). Bis-pyrazolone-based dysprosium(III) complexes: zero-field single-molecule magnet behavior in the [2 × 2] grid Dy$^{III}_4$ cluster. CrystEngComm. 2022;24(38):6688–6695.
Available:https://doi.org/10.1039/D2CE01067D

8. Aly AA, Abdallah EM, Ahmed SA, Rabee MM, Bräse, S. Transition Metal Complexes of Thiosemicarbazides, Thiocarbohydrazides, and Their Corresponding Carbazones with Cu(I), Cu(II), Co(II), Ni(II), Pd(II), and Ag(I)—A Review. Molecules. 2023;28(4):1808.
Available:https://doi.org/10.3390/molecules28041808

9. Kaya Y, Erçağ A, Uğuz, Ö, Zorlu Y, Koca A. Crystal structures, antioxidant, electrochemical and in-situ spectroelectrochemical properties of new bisthiocarbohydrazones and their Ni(II) complexes. Inorg. Chim. Acta. 2023; 549:121403.
Available:https://doi.org/10.1016/j.ica.2023.121403

10. Mikhailov OV, Chachkov DV. Molecular and Electronic Structures of Macrocyclic Compounds Formed at Template Synthesis in the M(II)—Thiocarbohydrazide—Diacetyl Triple Systems: A Quantum-Chemical Analysis by DFT Methods. Molecules. 2023;28(11):4383.

Available:https://doi.org/10.3390/molecules28114383

11. Potti ME, Kurup, MRPP, Fun, H-K. Macrocyclic molecular square complex of zinc(II) self-assembled with a carbohydrazone ligand. Inorg. Chem. Commun. 2007; 10(3):324–328.
Available:https://doi.org/10.1016/j.inoche.2006.11.009

12. Manoj E, Kurup MRP, Fun H-K, Punnoose, A. Self-assembled macrocyclic molecular squares of Ni(II) derived from carbohydrazones and thiocarbohydrazones: Structural and magnetic studies. Polyhedron. 2007;26(15):4451–4462.
Available:https://doi.org/10.1016/j.poly.2007.05.048

13. Shuvaev KV, Dawe LN, Thompson LK. Formation of unusual molecular rectangles and squares containing low spin and high spin Co(II) and Fe(II) centers. Dalton Trans. 2010;39(20):4768–4776.
Available:https://doi.org/10.1039/B915595C

14. Wu D-Y, Sato O, Einaga Y, Duan C-Y. A Spin-Crossover Cluster of Iron(II) Exhibiting a Mixed-Spin Structure and Synergy between Spin Transition and Magnetic Interaction. Angew. Chem. Int. Ed. 2009;48(8):1475–1478.
Available:https://doi.org/10.1002/anie.200804529

15. Mandal TN, Roy S, Konar S, Jana A, Ray S, Das K, Saha R, Fallah MSE, Butcher RJ, Chatterjee, S, Kar, SK. Self-assembled tetranuclear Cu$_4$(II), Ni$_4$(II) [2 × 2] square grids and a dicopper(II) complex of heterocycle based polytopic ligands - Magnetic studies. Dalton Trans. 2011;40(44): 11866–11875.
Available:https://doi.org/10.1039/C1DT10813A

16. Thompson, LK, Matthews, CJ, Zhao, L, Xu, Z, Miller, DO, Wilson, C, Leech, MA, Howard, JAK, Heath, SL, Whittaker, AG, Winpenny, REP. Synthesis, Structure, and Magnetism of a Series of Self-Assembled Polynuclear Mn(II), Co(II), and Cu(II) Cluster Complexes. J. Solid State Chem. 2001;159(2):308–320.
Available:https://doi.org/10.1006/jssc.2001.9160

17. Dawe, LN, Abedin, TSM, Kelly, TL, Thompson, LK, Miller, DO, Zhao, L, Wilson, C. Leech, MA, Howard, JAK. Self-assembled polymetallic square grids ([2 ×

2] M$_4$, [3 × 3] M$_9$) and trigonal bipyramidal clusters (M5)—structural and magnetic properties. J. Mater. Chem. 2006;16(26):2645–2659. Availablehttps://doi.org/10.1039/B602595A

18. Zhao L, Xu Z, Grove H, Milway VA, Dawe LN, Abedin TSM, Thompson, LK, Kelly, TM, Harvey, RG, Miller, DO, Weeks, L, Shapter, JG, Pope, KJ. Supramolecular Mn(II) and Mn(II)/Mn(III) Grid Complexes with [Mn$_9$(μ$_2$-O)$_{12}$] Core Structures. Structural, Magnetic, and Redox Properties and Surface Studies. Inorg. Chem. 2004;43(13):3812–3824. Available https://doi.org/10.1021/ic030319v

19. Garcia, AM, Romero-Salguero, FJ, Bassani, DM, Lehn, J-M, Baum, G, Fenske, D. Self-Assembly and Characterization of Multimetallic Grid-Type Lead(II) Complexes. Chem. - Eur. J. 1999;5(6):1803–1808 Available :https://doi.org/10.1002/(SICI)1521-3765(19990604)5:6<1803::AID-CHEM1803>3.0.CO;2-M

20. Dey, SK, Abedin, TSM, Dawe, LN, Tandon, SS, Collins, JL, Thompson, LK, Postnikov, AV, Alam, MS, Müller, P. Supramolecular Self-Assembled Polynuclear Complexes from Tritopic, Tetratopic, and Pentatopic Ligands: Structural, Magnetic and Surface Studies. Inorg. Chem. 2007;46(19):7767–7781. Available:https://doi.org/10.1021/ic070336a

21. Drover, MW, Tandon, SS, Anwar, MU, Shuvaev, KV, Dawe, LN, Collins, JL, Thompson, LK. Polynuclear complexes of a series of hydrazone and hydrazone–oxime ligands – M$_2$ (Fe), M$_4$ (Mn, Ni, Cu), and Mn (Cu) examples. Polyhedron. 2014;68:94–102. Available:https://doi.org/10.1016/j.poly.2013.10.018

22. Breuning, E, Hanan, GS, Romero-Salguero, FJ, Garcia, AM, Baxter, PNW, Lehn, J- M, Wegelius, E, Rissanen, K, Nierengarten, H, van Dorsselaer, A. Self-Assembly, Characterisation, and Crystal Structure of Multinuclear Metal Complexes of the [2×3] and [3×3] Grid-Type. Chem. - Eur. J. 2002;8(15):3458–3466. Available : https://doi.org/10.1002/1521-3765(20020802)8:15<3458::AID-CHEM3458>3.0.CO;2-Y

23. Xu Z, Thompson LK, Miller DO. A non-homoleptic Cu9 [3×3] mixed ligand grid—

structural and magnetic properties. Polyhedron. 2002;21(17):1715–1720. Available https://doi.org/10.1016/S0277-5387(02)01037-9

24. Babu CN, Sathyanarayana A, Mobin SM, Prabusankar G. Structurally characterized zwitterionic chiral zinc imidazolium [4,4] grid. Inorg. Chem. Commun. 2013;37:222–224. Available:https://doi.org/10.1016/j.inoche.2013.08.028

25. Dawe LN, Shuvaev KV, Thompson LK. (2009)Magnetic [n × n] (n = 2−5) Grids by Directed Self-Assembly. Inorga. Chem. 2009;48(8):3323–3341. Available:https://doi.org/10.1021/ic801078h

26. Seck TM, Diop M, Diouf D, Diouf O, Barry AH, Gaye, M. Synthesis, spectroscopic studies, and crystal structure determination of a tetranuclear Zn(II) [2x2] square grid structure of 1,5-bis(1-(pyridin-2-yl)ethylidene)carbonohydrazide. IOSJR J. Appl. Chem. 2018;11(12):06–14. Available: https://doi.org/10.9790/5736-1112010614

27. Sheldrick GM. SHELXT–Integrated space-group and crystal-structure determination. Acta Crystallographica Section A. 2015;71(1):3–8. Available :https://doi.org/10.1107/S2053273314026370

28. Sheldrick, GM. Crystal structure refinement with SHELXL. Acta Crystallographica Section C. 2015;71(1):3–8. Available :https://doi.org/10.1107/S2053229614024218

29. Farrugia LJ. WinGX and ORTEP for Windows: an update. J. Appl. Crystallogr. 2012;45(4):849–854. Available :https://doi.org/10.1107/S0021889812029111

30. Sow, MM, M, Diouf, O, Gaye M, Sall, AS, Castro G, Pérez-Lourido P, Valencia L, Sorace L. Sheets of Tetranuclear Ni(II) [2 × 2] Square Grids Structure with Infinite Orthogonal Two-Dimensional Water–Chlorine Chains. Cryst. Growth Des. 2013;13(10):4172–4176. Available :https://doi.org/10.1021/cg400885f

31. Geary, WJ. The use of conductivity measurements in organic solvents for the characterisation of coordination compounds. Coord. Chem. Rev. 1971; 7(1):81–122.

Available: https://doi.org/10.1016/S0010-8545(00)80009-0

32. Hossain SM, Lakma A, Pradhan RN, Demeshko, S, Singh AK. Valence directed binding mode of [2 × 2] iron grids of an unsymmetrical picolinic hydrazone based ligand. Dalton Trans. 2017;46(37):12612–12618.
Available:https://doi.org/10.1039/C7DT02433A

33. Pilichos E, Spanakis E, Maniaki EK, Raptopoulou CP, Psycharis V, Turnbull, MM, Perlepes, SP. Diversity of Coordination Modes in a Flexible Ditopic Ligand Containing 2-Pyridyl, Carbonyl and Hydrazone Functionalities: Mononuclear and Dinuclear Cobalt(III) Complexes, and Tetranuclear Copper(II) and Nickel(II) Clusters. Magnetochemistry. 2019;5(3): 39.
Available:https://doi.org/10.3390/magnetochemistry5030039

34. Glaser, T, Lügger, T. A new tetranuclear iron complex with a $[Fe_4O_6]^{6+}$ core: synthesis, structure, spectroscopic and magnetic properties. Inorg. Chim. Acta. 2002;337:103–112.

Available: https://doi.org/10.1016/S0020-1693(02)00989-1

35. Mitchell, KJ, Abboud, KA, Christou, G. (2016). Magnetostructural Correlation for High-Nuclearity Iron(III)/Oxo Complexes and Application to Fe_5, Fe_6, and Fe_8 Clusters. Inorg. Chem. 2016;55(13):6597–6608.
Available:https://doi.org/10.1021/acs.inorgchem.6b00769

36. Stamatatos TC, Escuer A, Abboud, KA, Raptopoulou CP, Perlepes SP, Christou G. Unusual Structural Types in Nickel Cluster Chemistry from the Use of Pyridyl Oximes: Ni_5, $Ni_{12}Na_2$, and Ni_{14} Clusters. Inorg. Chem. 2008;47(24): 11825–11838.
Available :https://doi.org/10.1021/ic801555e

37. Alexopoulou KI, Terzis A, Raptopoulou CP, Psycharis V, Escuer A, Perlepes, SP. Ni^{II}_{20} "Bowls" from the Use of Tridentate Schiff Bases. Inorg. Chem. 2015;54(12):5615–5617.
Available :https://doi.org/10.1021/acs.inorgchem.5b00521

Peer-review history:
The peer review history for this paper can be accessed here:
https://www.sdiarticle5.com/review-history/104173